Journal of
Materials Chemistry A

Accepted Manuscript

This is an *Accepted Manuscript*, which has been through the RSC Publishing peer review process and has been accepted for publication.

Accepted Manuscripts are published online shortly after acceptance, which is prior to technical editing, formatting and proof reading. This free service from RSC Publishing allows authors to make their results available to the community, in citable form, before publication of the edited article. This *Accepted Manuscript* will be replaced by the edited and formatted *Advance Article* as soon as this is available.

To cite this manuscript please use its permanent Digital Object Identifier (DOI®), which is identical for all formats of publication.

More information about *Accepted Manuscripts* can be found in the **Information for Authors**.

Please note that technical editing may introduce minor changes to the text and/or graphics contained in the manuscript submitted by the author(s) which may alter content, and that the standard **Terms & Conditions** and the **ethical guidelines** that apply to the journal are still applicable. In no event shall the RSC be held responsible for any errors or omissions in these *Accepted Manuscript* manuscripts or any consequences arising from the use of any information contained in them.

Cite this: DOI: 10.1039/c0xx00000x

www.rsc.org/xxxxxx

ARTICLE TYPE

Core-Shell, Hollow-Structured Iridium–Nickel Nitride Nanoparticles for the Hydrogen Evolution Reaction

Kurian A. Kuttiyiel, [a] Kotaro Sasaki,*[a] Wei-Fu Chen, [a] Dong Su, [b] and Radoslav R. Adzic *[a]

Received (in XXX, XXX) Xth XXXXXXXXX 20XX, Accepted Xth XXXXXXXXX 20XX

DOI: 10.1039/b000000x

We synthesized core-shell, hollow-structured iridium - nickel nitride nanoparticles and then evaluated their activity in the hydrogen evolution reaction (HER). Coupling Ni nitrides with the IrNi cores enhances the HER activity of Ir shells to a level comparable to that of Pt/C, while reducing the Ir loading of the catalyst.

The development of highly active, durable, and inexpensive catalysts for the hydrogen evolution reaction (HER) is one of the needs for the feasibility of the hydrogen-based economy.[1-3] Although Pt shows the highest activity for the HER, new electrode materials have been investigated, aiming at lowering costs. Core-shell structured nanoparticles have the potential to replace or reduce Pt in HER applications.[4-6] While a variety of carbon-supported Pt-group binary catalysts have been prepared by conventional methods, [7-11] as yet the ability to control the size, structure, and composition of core-shell nanoparticles is limited, for instance, due to the aggregation of metals at the nanoscale. Herein, we detail our demonstration of the synthesis of IrNiN core-shell and hollow nanoparticles by annealing them in an NH_3 environment. Our results showed that incorporating NiN into Ir changes the HER mechanism of Ir, thereby enhancing HER activity to a level comparable to that attained by Pt.

We synthesized carbon-supported IrNiN nanoparticles by chemical reduction using $NaBH_4$ and subsequently by thermal annealing using NH_3 as the nitrogen precursor at ambient pressure (see the ESI†). The mole ratio of Ir:Ni is 1:3. Fig. 1A shows a high-angle annular dark field (HAADF)–scanning transmission electron microscope (STEM) image of the IrNiN nanoparticles. These images revealed that generally the particles were spherical with an average diameter of 3.8 nm (Fig. S4 in the ESI†), which corresponds well the value we determined in the XRD experiments. We found that several large particles, varying in size between 12- to 25-nm were hollow structures, while most particles (> *ca* 90%) between 2- and 8-nm were solid ones. Fig. 1B exhibits the spectrum of electron energy loss spectroscopy (EELS) of the nitrogen K edge from the IrNiN sample. It clearly illustrates the incorporation of nitrogen in the nanoparticles. Fig. 1C is an HAADF image of a single hollow particle (14 nm in diameter). Such particles reveal a characteristic contrast difference between the center and the surrounding regions, i.e., the former are darker than the latter. Other examples of hollow structure are shown in Fig. S1 (ESI†). Fig. 1D represents an EELS intensity profile from the Ir M-edge and the Ni L-edge across the single hollow particle scanned along the line indicated in Fig. 1C. The resulting profile reveals that both the intensity of Ir and Ni in the center area is much lower than that in the surrounding area, confirming the formation of a hollow structure.

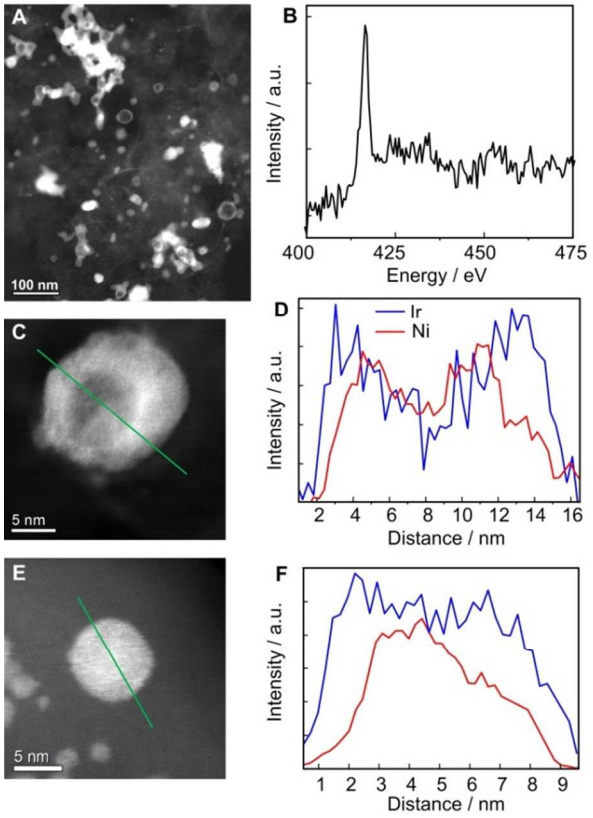

Fig. 1 (A) HAADF-STEM image of the IrNiN nanoparticles. (B) EELS spectrum of N K-edge in IrNiN nanoparticles. (C) and (E) HAADF-STEM images of representative hollow and core-shell IrNiN nanoparticles, respectively. (D) and (F) EELS intensities, respectively, for the Ir M-edge and Ni L-edge along the scanned line as indicated in (C) and (E).

Fig. 1F compares the EELS intensity from the Ir M-edge and the Ni L-edge across the single solid particle in Fig. 1E (diameter of 8 nm). In contrast to Figs. 1C and 1D, it is evident that the intensity of Ir is approximately constant around the centre of nanoparticle, while Ir is enriched (or Ni is depleted) at both edges of the nanoparticles; the thickness of the Ir-enriched layers is 1-3

nm. Hence, the STEM-EELS measurements demonstrate the formation of the core-shell structure for these relatively small nanoparticles. We note that an enrichment of Ir also is evident at the surfaces of the surrounding areas in the hollow particles (Fig. 1D)

X-ray diffraction (XRD) patterns (using Cu Kα radiation) of the H_2-reduced $IrNi_3$/C and the NH_3-treated $IrNi_3$/C samples are shown in Fig. 2A. The peaks in these samples lie between the 2θ angles of Ir (at the dotted red bars) and Ni (at the solid blue bars), but there are no clear separate peaks for each element. This finding implies that Ir and Ni form a solid-solution alloy. The interesting feature is that the NH_3 treatment induced a shift of the XRD peaks toward slightly lower angles compared with those of the H_2-treated sample, implying the formation of nitride, presumably Ni_4N, as is discussed below.

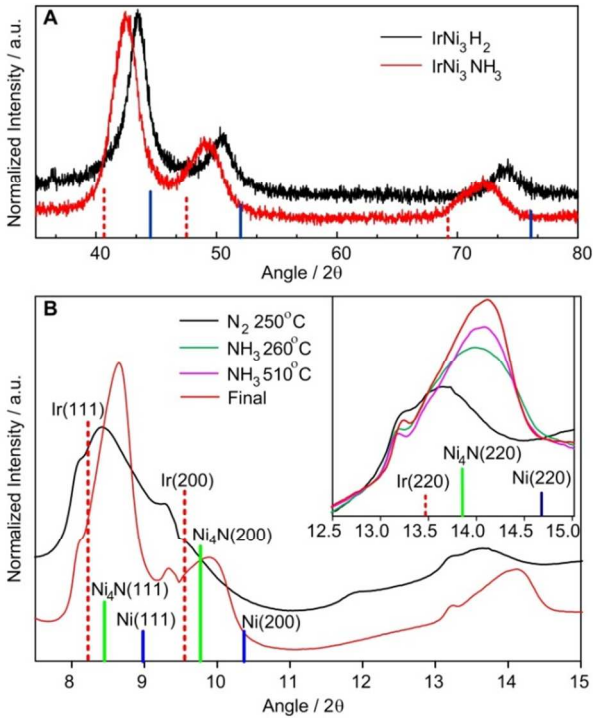

Fig. 2 (A) XRD patterns of carbon-supported $IrNi_3$ nanoparticles with Cu Kα radiation after annealing at 510°C in an atmosphere of H_2 and of NH_3 for 2 hours. The blue and green bars respectively designate the (111), (200), (220) reflections from pure Ir and Ni. The wavelength = 1.54056 Å. (B) Comparison of the synchrotron XRD patterns for $IrNi_3$ nanoparticles at 250°C in N_2 with 510°C in NH_3 showing the Ir and Ni_4N phases (red, green and blue bars designate the Ir, Ni_4N and Ni reflections, respectively). The inset shows the detailed patterns between 12.5° and 15° at different annealing temperatures. The wavelength = 0.3184 Å.

To study details of the formation of the core-shell structure during annealing in an NH_3 environment, we undertook synchrotron *in situ* time-resolved XRD measurements at beamline X7B in the NSLS, as shown in Fig. 2B and Fig. S2 (ESI†) (the wavelength: 0.3184 Å). We loaded the $IrNi_3$/C sample, reduced by $NaBH_4$ in a quartz reactor and annealed it from room temperature up to 250°C first in a flow of N_2 gas, followed by NH_3 gas, as depicted in the synthesis method (ESI†). The three major peaks shown in the figures became more intense as the temperature rose. The inset in Fig. 2B illustrates details of the *in situ* XRD patterns between (2θ =) 12.5° and 15.0° at different annealing temperatures and environments. Although the observed peaks lie between the reflections from Ir(220) and Ni(220) during the range of annealing temperatures, a distinct feature is noticeable, i.e., there is a significant shift in peak position towards a higher angle between N_2 at 250°C, and NH_3 at 260°C. This shift may reflect the incorporation of N due to the formation of Ni nitride under the NH_3 environment. Although two nitrides, Ni_3N and Ni_4N may be formed, we consider that it is likely to be Ni_4N, as there was no peak around 2θ = 11.6° for Ni_3N(112). The final peak in the inset of Fig. 2B is located at a slightly higher position than that of Ni_4N, suggesting that the cores may comprise both the IrNi solid solution and Ni_4N phases. (We note that the peaks would be at higher positions if the cores comprised only the IrNi solid solution alloy as discussed for the data shown in Fig. 2A.)

We further note that small peaks are seen at almost the same 2θs of pure Ir in the synchrotron XRD patterns. The peaks were present after the reduction by $NaBH_4$ and their intensity and positions did not change much during thermal annealing (see the ESI†), suggesting that a small number of Ir nanoclusters is formed by chemical reduction; nevertheless, they presumably are isolated ones, and, therefore, no growth or no alloying with Ni had taken place during the subsequent heat treatment. Furthermore, because of their low concentration, they have a negligible contribution to the HER, compared with the core-shell/hollow structured IrNiN nanoparticles.

The study of HER on the carbon-supported IrNiN-, Ir-, Ni-, and Pt-nanoparticles on a glassy carbon electrode was carried out at a potential sweep rate of 1 mV s^{-1} in an Ar-saturated 0.1 M $HClO_4$ solution (Fig. 3A). Ni/C consistently showed the most negative onset potential of an appreciable cathodic current density (green line). The polarization recorded with Ir/C revealed that the cathodic current rose rapidly beyond the zero overpotential (red line). By comparison, the same measurement, carried out for commercial Pt/C (E-TEK 10% Pt/C) produced an even steeper cathodic current beyond zero overpotential (black dash line). The i-V response of the IrNiN/C exhibited higher catalytic activity than that of Ir/C, and approached that of Pt/C (blue line). We determined the specific mass activity of these catalysts, as detailed in Table S1 (ESI†), by comparing the cathodic current density obtained at an overpotential of 0.1 V beyond the onset potential of HER. The IrNiN/C gave a specific Ir mass activity of 2.96 mA cm^{-2}, viz., 2.6 times higher than that of the Ir/C catalyst (1.15 mA cm^{-2}).

The polarisation curves recorded on IrNiN/C, Ir/C, Ni/C, and Pt/C (Fig. 3B) exhibited classical Tafel behavior, clearly indicating that the HER can be described by the Tafel equation (see the ESI†). The Tafel slope was calculated from the linear portion of the plot in the low overpotential region. The curves in the low current density region, illustrated in the figure, had Tafel slopes of 30.4, 36.0, 59.0 and 168.3 mV dec^{-1} for the Pt, IrNiN/C, Ir/C and Ni/C catalysts, respectively. The activity of IrNiN gave a Tafel plot very close to that of the Pt/C. The mechanism of the HER in acidic solution involves the discharge step (Volmer reaction), the electrochemical desorption step (Heyrovský reaction), and/or a recombination of two adsorbed hydrogen atoms (Tafel reaction). When the rate determining step (rds) is the Volmer reaction, the Tafel slope should be 116 mV dec^{-1}.

When Heyrovský reaction is the rds, the Tafel slope is 40 mV dec^{-1}, or 30 mV dec^{-1} for the Tafel reaction. Thus, the diagnostic criteria for the HER on Ir/C clearly demonstrate a Volmer-Heyrovský mechanism, i.e., the rate-controlling step is electrochemical desorption of H_{ads} and H_3O^+ to form hydrogen. The comparatively smaller Tafel slope of the IrNiN/C than that of the Ir/C demonstrates that the HER mechanism appears to alter as Ni nitride is incorporated. For the IrNiN/C, the low Tafel slope of 36.0 mV dec^{-1} suggests that the recombination of two adsorbed hydrogen atoms is accelerated on the surfaces of the Ir shell. Here, hydrogen evolution occurs via a Volmer-Tafel mechanism wherein the Tafel reaction is the rate-limiting step.

The exchange current density was obtained by measuring the current density in a narrow potential range ($\eta = \pm 5$ mV) near E_{eq} in a H_2-saturated 0.1 M $HClO_4$ solution. Herein, the Butler-Volmer equation can be expressed as $j=-j_0 nf\eta$.[14] The exchange current density was evaluated directly from the slope ($-j_0 nF/RT$) of the j-η curve (Fig. S3 in the ESI†). The IrNiN/C showed a j_o value of 0.613 mA cm^{-2} that is 22% lower than that of Pt/C, but 36% higher than that of Ir/C. This indicates that the intrinsic activity of Ir shell was enhanced by alloying with Ni and nitriding.

We attributed this enhancement in the HER to the down-shifting of the *d*-band center of Ir, through the contraction in Ir-Ir bond in the Ir shells. As the XRD studies demonstrated, nitriding shortens the Ir-Ir bond distance, while the Ni-Ni distance is lengthened. Similar phenomena were reported recently, showing that annealing IrNi nanoparticles beyond 450°C in H_2 results in Ir segregated to the surface of the IrNi solid alloy cores.[13] The down-shift of *d*-band centre may have two effects. One is that the surfaces become less reactive for H_2O oxidation and IrOH formation, so making the Ir shell surfaces more metallic, and accordingly, more active for hydrogen evolution. The other is to lower the hydrogen binding energy to a relatively moderate binding strength, which enhances the recombination of two H_{ads} atoms on the Ir surfaces.

In conclusion, we demonstrated that core-shell and hollow IrNiN nanoparticles have HER activity comparable to that of Pt/C. The incorporation of Ni nitrides to Ir changes the HER mechanism that is a consequence of the down-shifting of the *d*-band center of Ir on the surfaces.

This research was performed at BNL under contract DE-AC02-98CH10886 with the US Department of Energy.

Notes and references

[a] *Chemistry Department, Brookhaven National Laboratory, Upton, NY 11973, US. E-mail: ksasaki@bnl.gov, adzic@bnl.gov*
[b] *Center for Functional Nanomaterials, Brookhaven National Laboratory, Upton, NY 11973, US.*

† Electronic Supplementary Information (ESI) available: Detailed experimental procedures, See DOI: 10.1039/b000000x/

1. R. R. Adzic, *Frontiers in Electrochemistry*, VCH Publishers, New York, 1998.
2. W. Vielstich, A. Lamm and H. A. Gasteiger, *Handbook of Fuel Cells – Fundamentals, Technology and Applications*, John Wiley & Sons, Chichester, 2003.
3. W. F. Chen, K. Sasaki, C. Ma, A. I. Frenkel, N. Marinkovic, J. T. Muckerman, Y. M. Zhu and R. R. Adzic, *Angew Chem Int Edit*, 2012, **51**, 6131-6135.
4. D. V. Esposito, S. T. Hunt, A. L. Stottlemyer, K. D. Dobson, B. E. McCandless, R. W. Birkmire and J. G. G. Chen, *Angew Chem Int Edit*, 2010, **49**, 9859-9862.
5. I. J. Hsu, Y. C. Kimmel, X. G. Jiang, B. G. Willis and J. G. Chen, *Chem Commun*, 2012, **48**, 1063-1065.
6. J. Greeley, J. K. Norskov, L. A. Kibler, A. M. El-Aziz and D. M. Kolb, *Chemphyschem*, 2006, **7**, 1032-1035.
7. S. Yamamuro and K. Sumiyama, *Chem Phys Lett*, 2006, **418**, 166-169.
8. W. M. Wang, D. Zheng, C. Du, Z. Q. Zou, X. G. Zhang, B. J. Xia, H. Yang and D. L. Akins, *J Power Sources*, 2007, **167**, 243-249.
9. E. Antolini, *Mater Chem Phys*, 2003, **78**, 563-573.
10. L. Xiong and A. Manthiram, *Electrochim Acta*, 2005, **50**, 2323-2329.
11. L. Zhang, K. C. Lee and J. J. Zhang, *Electrochim Acta*, 2007, **52**, 7964-7971.
12. B. D. Cullity, *Elements of x-ray diffraction*, Prentice-Hall Inc., New York, 2001.
13. K. Sasaki, K. A. Kuttiyiel, L. Barrio, D. Su, A. I. Frenkel, N. Marinkovic, D. Mahajan and R. R. Adzic, *J Phys Chem C*, 2011, **115**, 9894-9902.
14. A. J. Bard and L. R. Faulkner, *Electrochemical methods: fundamentals and applications*, John Wiley & Sons, New York, 2001.

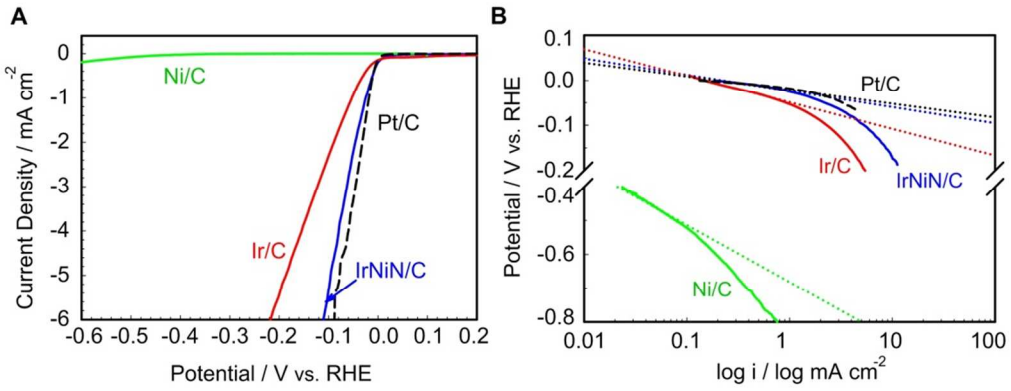

Fig. 3 (A) The polarization curves and (B) the corresponding Tafel plots of IrNiN/C, Ir/C, Ni/C and Pt/C catalysts in a 0.1M $HClO_4$ solution.